Scilight

Regenerative Medicine and Dentistry

https://www.sciltp.com/journals/rmd



Article

Check for updates

Comparative Effects of 808 nm Laser and Multi-Wavelength Near-Infrared Photobiomodulation on Osteogenic Protein-Associated Fluorescence in MG-63 Osteoblast-Like Cells

Simone L. Sleep [1], Deanne Hryciw [2,3], Eliza Ranjit [1], Laurence J. Walsh [4], Nifty Tomy [5] and Roy George [1,*]

[1] School of Medicine and Dentistry, Griffith University, Gold Coast Campus, Brisbane, QLD 4215, Australia
[2] School of Environment and Science, Griffith University, Brisbane, QLD 4111, Australia
[3] Institute for Biomedicine and Glycomics, Griffith University, Brisbane, QLD 4111, Australia
[4] School of Dentistry, The University of Queensland, Herston, QLD 4006, Australia
[5] Cochin Cancer Research Centre, North Kalamassery, Kerala 683503, India
* Correspondence: r.george@griffith.edu.au; Tel.: +61-(0)7-5678-0751

How To Cite: Sleep, S.L.; Hryciw, D.; George, R.; et al. Comparative Effects of 808 nm Laser and Multi-Wavelength Near-Infrared Photobiomodulation on Osteogenic Protein-Associated Fluorescence in MG-63 Osteoblast-Like Cells. *Regenerative Medicine and Dentistry* **2026**, *3* (4), 15. https://doi.org/10.53941/rmd.2026.100015

Received: 22 July 2026
Revised: 8 October 2026
Accepted: 14 October 2026
Published: 30 October 2026

Abstract: Introduction: This study, for the first time, investigated the effects of polychromatic multi-wavelength near-infrared (PMNI) photobiomodulation (PBM) on osteoblast-associated protein fluorescence in MG-63 osteoblast-like cells, examining the relationship between exposure, timing (immediate and 24 h post-treatment), and irradiation wavelength. Specifically, cells were exposed to a proprietary blend of light-emitting diodes (wavelengths 775, 845 and 940 nm) or to a single-wavelength 808 nm diode laser. **Methods:** MG-63 osteoblast-like cells were exposed to the multi-wavelength LED for 30 or 60 s or to the 808 nm diode laser for 33 or 100 s. Protein-associated fluorescence was assessed immediately and 24 h following irradiation. Immunofluorescence intensity for alkaline phosphatase (ALP), RUNX2, BMP-2, COL-1, OPN and OCN was quantified using ImageJ software (version 1.54t). **Results:** PMNI-LED increased osteogenic protein-associated fluorescence across all six markers under at least one irradiation condition, with the largest response observed for BMP-2 following 30 s irradiation assessed immediately. The magnitude and direction of responses varied according to exposure duration and assessment time. In contrast, the 808 nm laser produced a more selective response pattern, with persistent reductions in ALP and RUNX2 fluorescence, increases in OPN under several irradiation conditions, and smaller marker-specific increases in BMP-2, OCN and COL-1. **Conclusion:** MG-63 osteoblast-like cells respond to photobiomodulation with near-infrared light from both polychromatic LED and single diode light sources. The fluorescence intensity associated with osteogenic protein markers was influenced by wavelength composition, radiant exposure and assessment time following PBM therapy.

Keywords: photobiomodulation; LED; multi-wavelength; Osteogenesis; MG-63; bone healing

1. Introduction

Photobiomodulation (PBM) has emerged as a promising technique for stimulating various biological processes involved in tissue regeneration, including angiogenesis, osteogenic differentiation, and wound healing [1,2]. For

Copyright: © 2026 by the authors. This is an open access article under the terms and conditions of the Creative Commons Attribution (CC BY) license (https://creativecommons.org/licenses/by/4.0/).
Publisher's Note: Scilight stays neutral with regard to jurisdictional claims in published maps and institutional affiliations.

example, PBM has been reported to upregulate expression of bone morphogenetic proteins (BMP) [3], which are key signalling molecules for cellular differentiation [4,5]. PBM employs light sources that emit one or more wavelengths, typically within the visible red or near-infrared spectrum, using lasers or light-emitting diodes (LEDs) to activate different biological pathways.

PBM, when applied using appropriate parameters, may enhance osteoproliferation and osteoinduction and support socket bone preservation following tooth extraction [6]. Lima et al. (2020) suggested that the use of multiple wavelengths may provide advantages over single-wavelength irradiation for bone healing and regeneration [2]. Recent studies have demonstrated the efficacy of polychromatic multi-wavelength near-infrared (PMNI-LED) devices for other applications such as dental analgesia, with some studies reporting greater analgesic effects than single-wavelength near-infrared diode lasers [7]. Near-infrared PBM is thought to interact with wavelength-dependent cellular photoacceptors and signalling pathways, including mechanisms involving cytochrome c oxidase, nitric oxide and reactive oxygen species [8,9].

The MG-63 osteoblast-like cell line is used extensively to study bone development, bone cell viability, and osteoblast differentiation in bone tissue engineering studies [10]. These cells are known for their stability and consistent responses, even after multiple passages in culture [11]. These cells can respond to near-infrared PBM, with altered mitochondrial activity, ATP production and ROS signalling [9]. PBM can also influence MG-63 expression of osteogenic markers, including osteocalcin (OCN), type I collagen (COL-1), RUNX2 transcription factor and BMP-2 at the gene level [12,13].

Past PBM studies suggest that when using single-wavelength light sources, multiple low-dose treatments may be more effective for promoting bone regeneration than a single dose [14]. Whether the same approach holds true for PMNI-LED light sources administered to bone-forming cells remains to be investigated. Given this background, this is the first study to utilise a proprietary PMNI-LED device in MG-63 osteoblast-like cells and compare its effects with those of a single-wavelength 808 nm diode laser. The study assessed PBM responses of MG-63 osteoblast-like cells in terms of six markers of bone repair and formation, both immediately after PBM, and after 24 h, using two different exposure settings.

2. Materials and Methods

2.1. Cell Culture

MG-63 cells (ATCC CRL-1427, passage 8) were obtained directly from the American Type Culture Collection (ATCC). MG-63 is a human osteosarcoma-derived, osteoblast-like cell line commonly used as a standardised model of osteoblastic responses [10,11]. MG-63 osteoblast-like cells were selected as a reproducible osteoblast-like model suitable for controlled exposure–response investigations, minimising biological variability between experimental groups. The cells were grown in T75 flasks using Dulbecco's Modified Eagle's Medium (GIBCO; Invitrogen, Carlsbad, CA, USA) with 10% fetal calf serum and 1% penicillin-streptomycin, at 37 °C in an atmosphere of 5% CO^2. The 7-day pre-treatment period was selected because of the low initial seeding density, allowing sufficient cell attachment, proliferation and establishment of cell-to-cell contact before PBM exposure while avoiding premature confluence. Once the cells reached full confluence, they were detached using 0.05% trypsin/EDTA and plated onto black-walled microplates (Corning® 384-well, #CLS4514), keeping each treatment group separate. These plates had low volume wells with a diameter of 3.6 mm and a depth of 11 mm. The black areas served as optical barriers and prevented light from spreading into adjacent wells.

Cells were plated at a low cell density of 30–50 cells per well. This low density was chosen to prevent the cells from reaching confluence in the small well. This approach minimised bias and accounted for spatial variability across the cell population. The plates were then incubated for 7 days before PBM treatments.

2.2. Light Sources for PBM

Details of the PMNI-LED light source and the reference diode laser are given in Table 1. The PMNI-LED device had three emission peaks at 775 nm, 845 nm and 940 nm, representing 40%, 45%, and 15%, respectively, of the total optical output, according to manufacturer specifications. Because the wavelengths were emitted simultaneously, optical output was additionally characterised experimentally using an Ophir power meter under the culture-plate and culture-medium conditions used for PBM treatment shown in Table 2.

The 808 nm diode laser used an optical fibre/Cap-B probe with an 8 mm external diameter, while the PMNI-LED device used a multi-core glass rod with an 8 mm external diameter. The terminal end of the light delivery system was positioned on the surface of the well. The optical emissions from the delivery system were measured using a laser power meter with an external sensor (Nova II, Ophir Optronics Solutions Ltd., Jerusalem, Israel), with the laser power meter set to different nominal wavelengths across the emitted range (Table 1).

Previous experiments validated photonic transmission by measuring optical power beneath the culture plates and in adjacent wells to assess both transmitted light and potential leakage between wells [15–17]. Measurements confirmed transmission of optical energy through the culture system, while no detectable energy was recorded in adjacent wells, demonstrating effective optical isolation between treatment conditions For the PMNI-LED device, measured power beneath culture wells was slightly greater in the presence of culture medium than in empty wells, whereas the 808 nm laser demonstrated attenuation following transmission through the culture system. Detailed measurements of optical power, radiant energy and radiant exposure delivered beneath the culture wells are presented in Table 2.

The PMNI-LED device was firmly secured using a clamp stand to ensure the terminal end of the light delivery system remained perpendicular and flush with the top surface of each well. The beam spot size for both devices was 7.0 mm in diameter (area: 0.39 cm^2). The glass rod tip was positioned 1 mm above the cell culture medium. The tip had a divergence angle of 70.9° in air (35.45° × 2) and a refractive-index-corrected divergence angle of 53.4° (26.7° × 2) in DMEM medium (refractive index ~1.33), which narrows the beam spread due to refraction. Both devices had spots with a Gaussian beam profile, with peak intensity at its centre, gradually decreasing toward the edges. The beam's full width at half maximum (FWHM) measured 3.0 mm. As a result, a central zone of 3.81 mm diameter at the bottom of the well received a consistent photon flux in a manner suitable for monolayer cell irradiation. On day 7 after seeding, when MG-63 osteoblast-like cells had reached cell-to-cell contact, cells received a single PBM treatment using either PMNI-LED (30 or 60 s) or an 808 nm diode laser (33 or 100 s). A schematic overview of the PBM treatment protocol and assessment time points is shown in Figure 1. Protein-associated fluorescence was assessed immediately (within 15 min) or after 24 h. Untreated controls were included at each assessment time point. Quantitative fluorescence analysis was performed on images acquired from treated cultures.

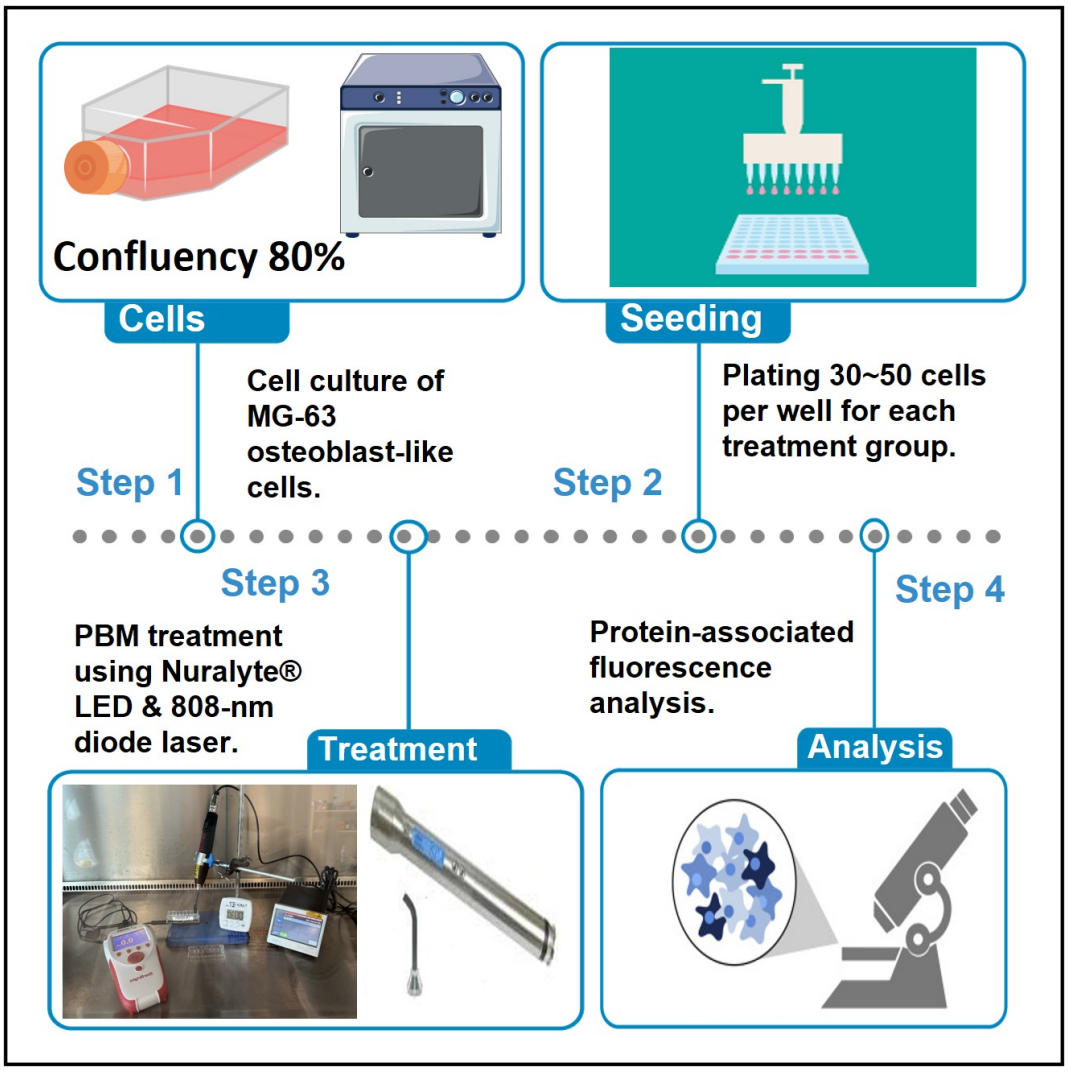


Figure 1. Schematic diagram showing photobiomodulation treatments of MG-63 osteoblast-like cells with single and multi-wavelength (polychromatic) PBM devices.

Table 1. Irradiation parameters and optical characteristics of the 808 nm diode laser and multi-wavelength near-infrared LED used for PBM.

Parameter	808 nm Diode Laser	PMNI-LED
Device	KLAS-DX82 diode laser	Nuralyte™ multi-wavelength LED
Manufacturer	Konftec, New Taipei City, Taiwan	Dentroid Pty Ltd., Canberra, Australia
Emission wavelength(s)	808 nm	775, 845 and 940 nm
Mode of operation	Continuous wave	Continuous wave
Application	Non-contact	Non-contact
Delivery system	Optical fibre/Cap-B probe 8 mm	Optical multi-core glass rod, 8 mm external diameter
Beam spot diameter at culture well	7.0 mm	7.0 mm
Beam spot area	0.39 cm^2	0.39 cm^2
Exposure duration	33 and 100 s	30 and 60 s
Nominal/device setting	5 and 15 J	700 mA
Average power	0.225 W	775 nm: 0.335 W; 845 nm: 0.450 W; 940 nm: 0.620 W *
Measured radiant energy	33 s: 7.3 J; 100 s: 22.0 J	775 nm: 11.0 J ** (30 s), 22.0 J (60 s); 845 nm: 13.3 J (30 s), 27.0 J (60 s); 940 nm: 3.7 J (30 s), 7.5 J (60 s)
Pulse frequency	Not applicable—continuous wave	Not applicable—continuous wave

Note: * Manufacturer/device output specification (W); ** Ophir-derived measured radiant energy (J).

Table 2. Optical characterisation of 810nm Laser and PMNI-LED irradiation through the cell-culture system.

Wavelength (nm)		Exposure Time (s)	Measured Power		Radiant Energy		Radiant Exposure	
			Clear Plate Only (W)	Plate + Medium (W)	Plate Only (J)	Plate + Medium (J)	Plate Only (J/cm^2)	Plate + Medium (J/cm^2)
PMNI-LED	775	30	0.0626	0.066	1.878	1.98	4.82	5.08
	775	60	0.0626	0.066	3.756	3.96	9.63	10.15
	845	30	0.0773	0.0891	2.319	2.673	5.95	6.85
	845	60	0.0773	0.0891	4.638	5.346	11.89	13.71
	940	30	0.1083	0.1326	3.249	3.978	8.33	10.2
	940	60	0.1083	0.1326	6.498	7.956	16.66	20.4
Laser	808	33	0.1470	0.0708	4.851	2.336	12.44	5.99
	808	100	0.1470	0.0708	14.700	7.080	37.69	18.15

2.3. Immunocytochemistry/Fluorescence Analysis

Osteogenic protein-associated fluorescence for OCN, OPN, ALP, RUNX2, COL-1 and BMP-2 was evaluated using immunofluorescence, as described previously [18]. Cells were fixed with 4% paraformaldehyde for 45 min and then blocked and permeabilised with 0.3% Triton-X and 3% bovine serum albumin in phosphate-buffered saline for 30 min. After washing, were incubated with the appropriate primary antibodies at 4 °C for 24 h. The optimal concentrations of the primary antibodies (ALP 1:100, ab65834, Abcam, UK; OCN 1:500, ab93876, Abcam, UK; OPN 1:100, ab283656, Abcam, UK; BMP-2 1:500, ab214821, Abcam, UK; COL-11:500, ab138492, Abcam, UK; and RUNX2 1:500, ab192256, Abcam, UK) were previously determined by titration. After washing, the cells were then incubated a 1:500 mixture of the secondary antibody (donkey anti-rabbit IgG-Alexa Fluor™ 647, Invitrogen, Thermo Fisher Scientific) and stained with 10 µM bisBenzimide H 33342 trihydrochloride (Hoechst, Sigma Aldrich, cat. #33342) for 1 h in the dark. Digital fluorescence images were acquired using a Nikon Ti2 inverted microscope with a 10× objective and analysed using ImageJ® software (version 1.54t, NIH, Bethesda, MD, USA) [19]. Fluorescence intensity was used as a relative measure of antibody-associated protein signal. For each treatment condition, three microscopic fields of view containing approximately 20–30 cells per field were analysed, and the resulting measurements were averaged to obtain a mean fluorescence value for that condition.

2.4. Data Analysis

Descriptive analyses and graphical presentations were performed using GraphPad Prism 11.1.0 (GraphPad Software, San Diego, CA, USA). Immunofluorescence data were expressed as percentage and fold change relative to untreated controls. Exposure-response contrast was calculated as the difference in percentage change between higher and lower exposure conditions. Because only aggregated condition-level fluorescence measurements were available in the archived dataset, the immunofluorescence analysis was descriptive in nature, focusing on the magnitude and direction of treatment-associated responses rather than formal statistical inference. Values are presented as mean ± standard deviation (SD) for the three microscopic fields. The SD was calculated from three equal, non-overlapping regions of each analysed fluorescence image and therefore represents within-image spatial variability rather than variability between independent biological replicates.

3. Results

3.1. Osteoblast-Associated Protein Fluorescence after PMNI-LED PBM

Protein-associated fluorescence after PMNI-LED irradiation is summarised in Figures 2A and 3, and Table 3. PMNI-LED produced marker- and condition-dependent changes in protein-associated fluorescence. BMP-2 increased under all tested PMNI conditions, with the largest increase following 30 s irradiation assessed immediately (+306%). COL-1 showed its largest increase following 60 s irradiation assessed immediately (+121%), while OCN increased by 46% at 24 h following 60 s irradiation. ALP and RUNX2 increased by 34% and 27%, respectively, following 60 s irradiation assessed immediately, while OPN showed a smaller increase of 17%. Reductions were observed for several markers under other irradiation conditions.

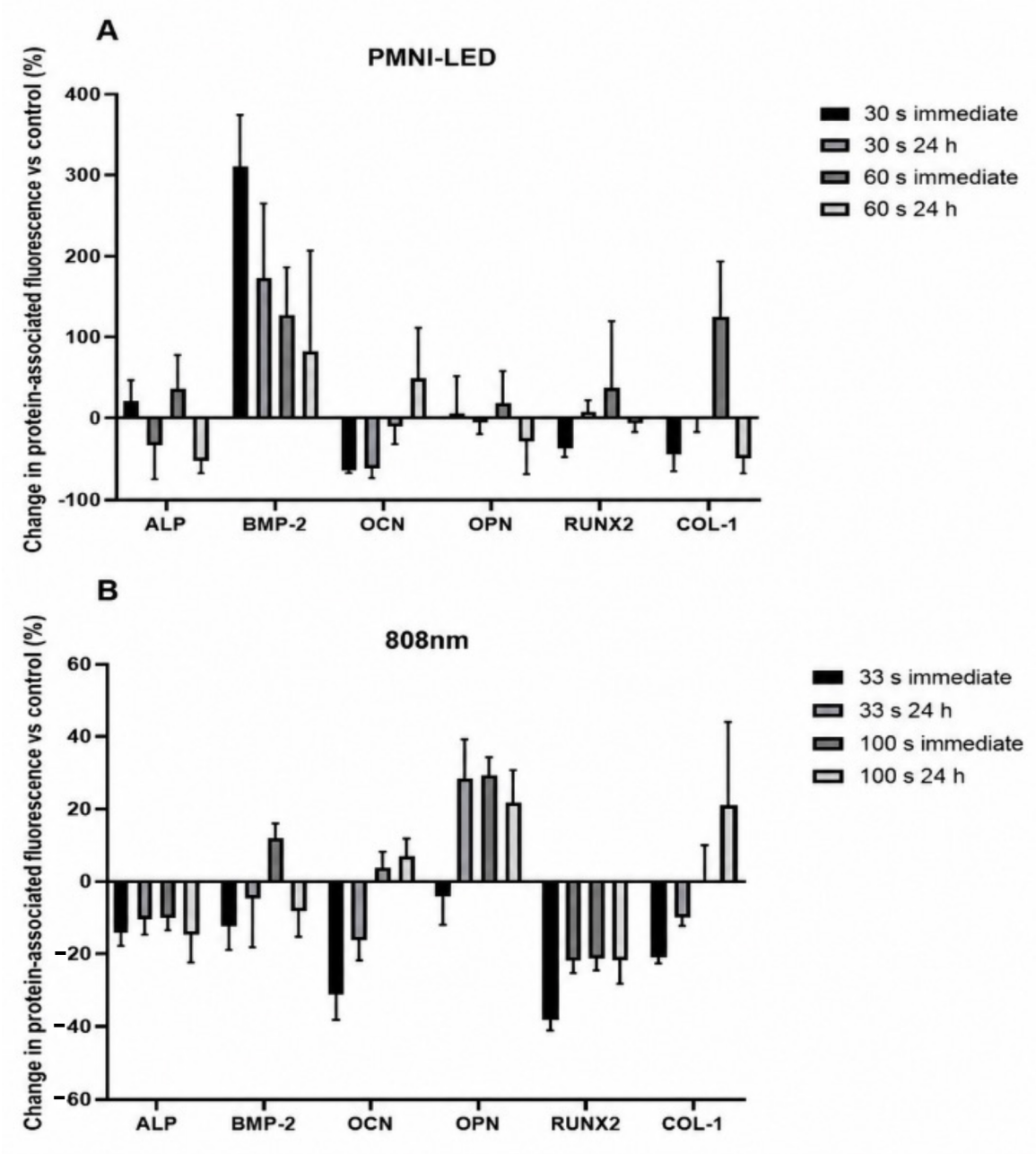


Figure 2. Percentage change in protein-associated fluorescence relative to untreated control. (**A**) PMNI-LED treatment following 30 or 60 s irradiation, assessed immediately and at 24 h. (**B**) 808 nm diode laser treatment following 33 or 100 s irradiation, assessed immediately and at 24 h. Values represent descriptive percentage change calculated from the mean fluorescence intensity of three microscopic fields per condition. Untreated control was defined as 0% change. No inferential statistical comparisons are shown. Bars represent mean percentage change relative to untreated control, with error bars showing SD calculated from three equal, non-overlapping image regions. These regions represent technical/spatial subsamples rather than independent biological replicates.

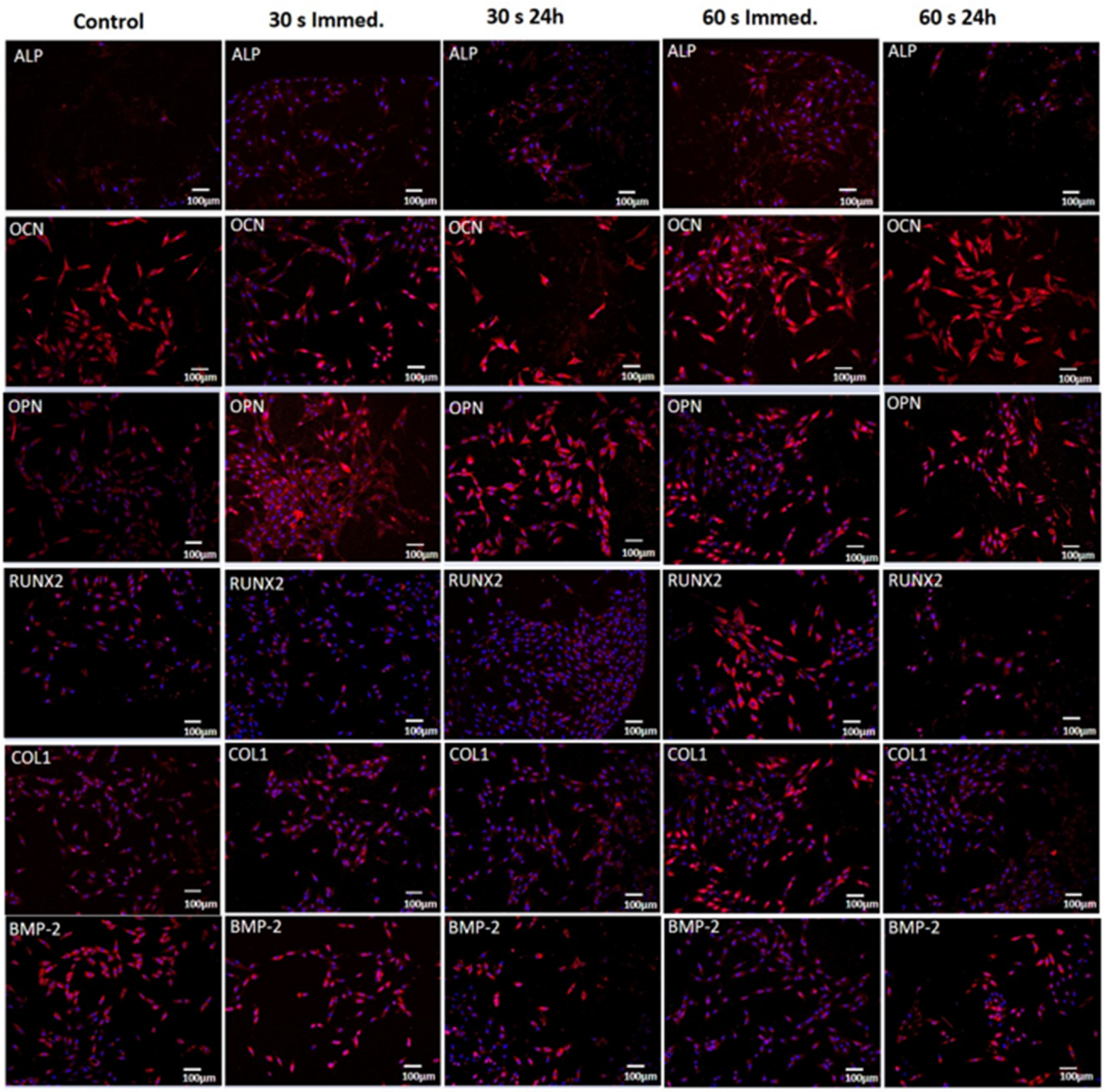


Figure 3. Representative immunofluorescence images of MG-63 osteoblast-like cells following PMNI-LED PBM. Immunofluorescence of MG-63 osteoblast-like cells at baseline (control, left column), and after PMNI-LED irradiation for either 30 s or 60 s, when assessed immediately or after 24 h. Osteogenic markers are shown in red (Alexa Fluor-647), while cell nuclei are shown in blue (Hoechst 33342). Images were acquired using a 10× objective. Scale bar indicates 100 μm. These are representative fluorescence images from the analysed samples.

Table 3. Exposure–response percentage change in protein-associated fluorescence relative to control.

	PMNI-LED Exposure–Response (%)			
	30 s Immed.	**30 s 24 h**	**60 s Immed.**	**60 s 24 h**
ALP	+19%	−34%	+34%	−53%
BMP-2	+306%	+171%	+125%	+79%
OCN	−63%	−61%	−12%	+46%
OPN	+5%	−6%	+17%	−30%
RUNX2	−41%	+1%	+27%	−13%
COL-1	−46%	−1%	+121%	−50%
	808 nm laser exposure–response (%)			
	33 s Immed.	**33 s 24 h**	**100 s Immed.**	**100 s 24 h**
ALP	−14%	−10%	−10%	−15%
BMP-2	−13%	−5%	+12%	−8%
OCN	−31%	−16%	+4%	+7%
OPN	−4%	+29%	+29%	+22%
RUNX2	−38%	−22%	−21%	−22%
COL-1	−21%	−10%	0%	+21%

3.2. Protein-Associated Fluorescence after Single-Wavelength PBM Using an 808 nm Diode Laser

Changes in protein-associated fluorescence following diode laser PBM are shown in Figures 2B and 4, and Table 3. The 808 nm diode laser produced a more selective, condition-dependent pattern. ALP and RUNX2 fluorescence remained below control across all irradiation conditions. OCN decreased following 33 s irradiation but was close to or slightly above control following 100 s irradiation. OPN increased at 24 h following 33 s irradiation and both immediately and at 24 h following 100 s irradiation. BMP-2 showed a modest increase following 100 s irradiation assessed immediately, while COL-1 increased at 24 h following 100 s irradiation.

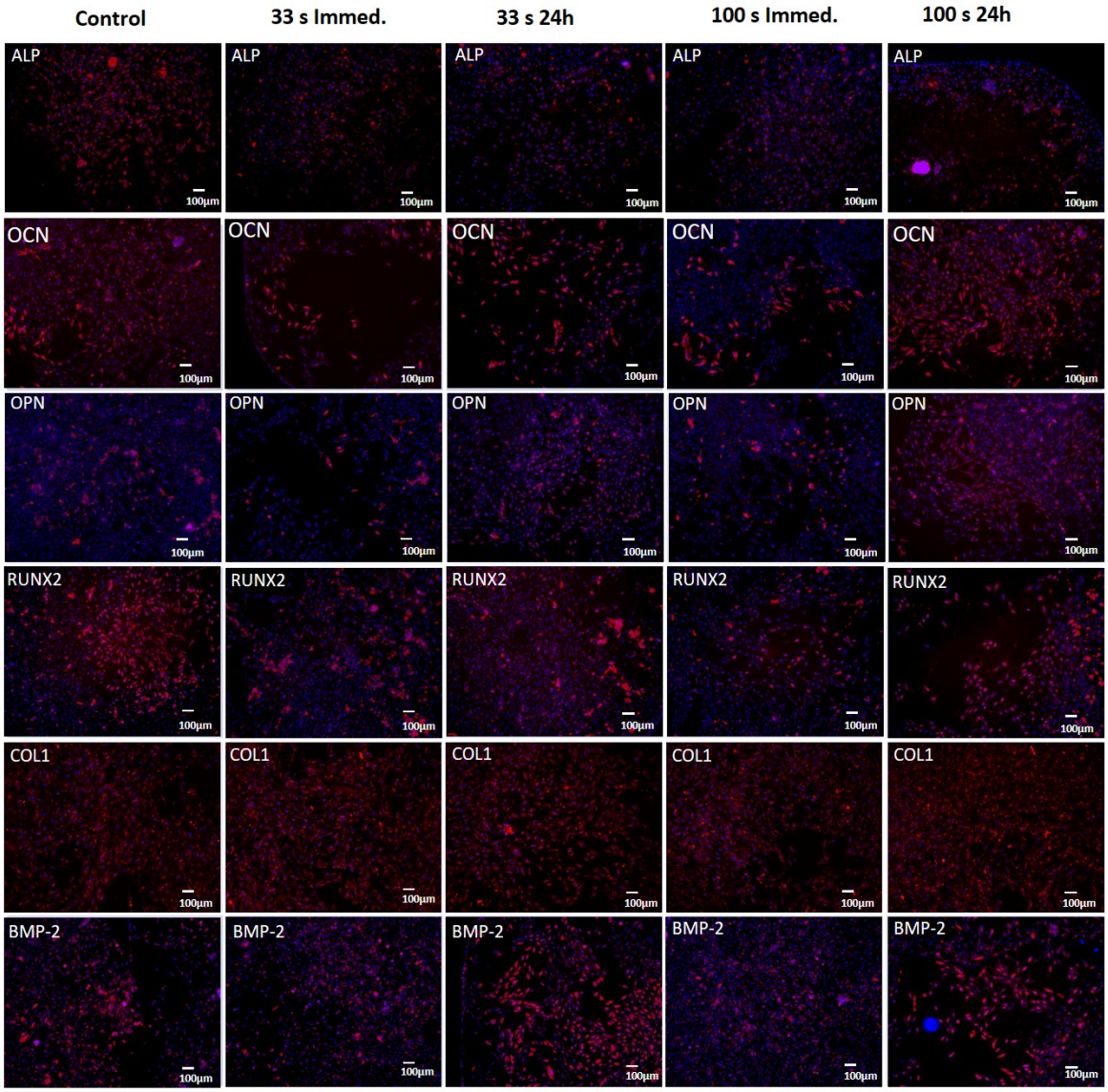


Figure 4. Representative immunofluorescence images of MG-63 osteoblast-like cells after single-wavelength PBM**.** This composite image is presented in the same format as Figure 3, with the baseline (control) as the left column, followed by laser PBM groups when assessed immediately or after 24 h. Images were acquired using a 10× objective. These are representative fluorescence images from the analysed samples.

3.3. Exposure-Response Contrast Analysis

Exposure-response contrast analysis demonstrated marker-specific differences according to light source and assessment time (Table 4). Positive contrast values indicate greater fluorescence at the higher exposure condition, whereas negative values indicate greater fluorescence at the lower exposure condition. For both light sources, exposure-response relationships varied between the immediate post-treatment assessment and the 24 h assessment, indicating time-dependent differences in protein-associated fluorescence responses.

Table 4. Exposure-response contrast (%) between low- and high-exposure conditions at immediate and 24 h post-treatment assessments.

Protein	PMNI-LED Immediate (60 s–30 s)	PMNI-LED 24 h (60 s–30 s)	808 nm Laser Immediate (100 s–33 s)	808 nm Laser 24 h (100 s–33 s)
ALP	15	−19	4	−5
BMP-2	−181	−92	25	−3
OCN	51	107	35	23
OPN	12	−24	33	−7
RUNX2	68	−14	17	0
COL-1	167	−49	21	31

4. Discussion

The findings extend current understanding of how near-infrared PBM modulates osteoblast-associated proteins in MG-63 osteoblast-like cells. To our knowledge, this is the first study to compare PMNI-LED and 808 nm diode-laser PBM using quantitative immunofluorescence of osteogenic protein markers as the primary endpoint. Distinct response patterns were observed according to light source, irradiation condition and post-treatment assessment time.

Osteogenic protein-associated fluorescence was modulated by both light sources, although the response patterns differed. PMNI-LED produced increased fluorescence for all six markers under at least one irradiation condition, with changes in BMP-2 and COL-1 evident at the shortest exposure time and earliest assessment point. These early effects likely reflect protein release or reorganisation rather than de novo protein synthesis [9]. Changes observed within approximately 15 min of PBM are unlikely to be explained solely by de novo protein synthesis. They may reflect rapid changes in protein localisation, turnover, conformation, epitope accessibility or other cellular processes; however, these mechanisms were not directly assessed.

In contrast, changes observed in fluorescence intensity at 24 h after PBM are more likely to reflect changes in downstream cellular signalling, including new protein synthesis and/or post-translational modifications. MG-63 osteoblast-like cells cultured on polystyrene have a reported population-doubling time of approximately 29.5 ± 3.7 h under standard culture conditions [20]. Consequently, changes in cell number or density over the 24 h assessment period cannot be excluded as a potential contributor and were not independently quantified in the present study.

PMNI-LED PBM increased fluorescence intensity associated with multiple osteogenic markers at 24 h, including ALP, BMP-2, OCN, RUNX2, and COL-1. In contrast, PBM using a single-wavelength 808 nm diode laser produced a more limited and selective response, characterised by increased fluorescence of BMP-2 and OPN alongside decreased fluorescence of ALP, OCN, and RUNX2. These treatment-specific patterns are compatible with a role for wavelength composition, but the differences cannot be attributed to wavelength composition alone because the irradiation conditions were not dosimetrically matched.

Under the irradiation conditions tested, PMNI-LED irradiation produced larger response contrasts and fold changes across several osteogenic proteins than the 808 nm diode laser, particularly for OCN and COL-1, indicating broader modulation of proteins associated with matrix maturation and formation. The broader activation profile observed following PMNI-LED irradiation may be explained by simultaneous interaction of light with multiple photoacceptors, resulting in modulation of more signalling processes than would occur with single-wavelength irradiation [2,8,21]. The present findings that the 808 nm diode laser produced a more selective pattern of protein modulation, primarily affecting BMP-2 and OPN, are consistent with wavelength-dependent cellular responses reported previously for 808 nm PBM [22].

The study was designed to characterise early changes in osteoblast-associated protein fluorescence following PBM rather than functional osteogenic differentiation. Consequently, cells were not cultured under osteogenic induction conditions, and assessment was limited to immediate and 24 h responses. Early fluorescence changes are likely to reflect alterations in protein localisation, turnover, conformation or release, whereas changes observed at 24 h may additionally reflect downstream signaling and protein synthesis. However, whether these responses translate into enhanced osteogenic differentiation, extracellular matrix mineralisation or bone formation remains uncertain [12,23,24].

Future studies should include functional endpoints such as ALP activity, extracellular matrix mineralisation and longer-term differentiation assays, with three-dimensional or in vivo models used to evaluate biological relevance [13,25]. Evaluation of a broader range of irradiation parameters would also help characterise potential biphasic dose-response behaviour reported for PBM [26–28]. Although previous clinical and preclinical studies suggest that PBM may influence tissue repair and bone healing, findings remain variable [29–34]. The present

results therefore provide mechanistic data supporting further investigation rather than direct evidence of enhanced osteogenesis.

Clinical studies evaluating PBM in oral and maxillofacial applications have reported mixed outcomes, including improvements in soft-tissue healing, implant stability and periodontal regeneration, but less consistent effects on radiographic bone repair [31–34]. Accordingly, the present findings should be interpreted as evidence of early molecular responses to PBM rather than direct evidence of enhanced bone regeneration.

A further limitation was the use of MG-63 cells, an osteosarcoma-derived osteoblast-like model that does not fully reproduce primary human osteoblast biology. MG-63 cells were selected as a standardised model to reduce donor-to-donor variability, improve experimental reproducibility and enable controlled evaluation of exposure–response effects. However, future studies using primary human osteoblasts or mesenchymal stem cell-derived osteoblasts are warranted to confirm the translational relevance of these findings.

Because the two PBM devices differed in wavelength composition, exposure duration and radiant exposure, the present study was not designed as a dosimetrically matched comparison; therefore, differences between devices should be interpreted as treatment-specific response patterns rather than evidence of intrinsic superiority of one light source.

5. Conclusions

The present results demonstrate that, under the irradiation conditions examined, multi-wavelength PBM produced broader modulation of osteoblast-associated protein fluorescence in MG-63 osteoblast-like cells than the single-wavelength 808 nm laser. These findings indicate that osteoblast-associated fluorescence responses vary according to light source, irradiation condition and post-treatment assessment time. Further studies using direct protein quantification methods and functional osteogenic assays are required to determine whether the observed changes in immunofluorescence signals translate into enhanced osteogenic differentiation and bone formation.

Author Contributions

S.L.S., D.H., L.J.W., E.R., N.T. and R.G. contributed to the conception and design of the study, data acquisition, analysis and interpretation, and drafting or critical revision of the manuscript. S.L.S, E.R. and R.G. contributed to immunofluorescence data acquisition and fluorescence image analysis; N.T. contributed to data analysis; and S.L.S., L.J.W., R.G., D.H. and E.R. contributed to data analysis and interpretation, and critical revision of the manuscript. All authors have read and agreed to the published version of the manuscript.

Funding

This research received no external funding.

Institutional Review Board Statement

This study involved the MG-63 osteoblast-like cell line and did not involve human participants or animals. No institutional ethics approval was required.

Informed Consent Statement

Not applicable.

Data Availability Statement

The original contributions presented in the study are included in the article, and further inquiries can be directed to the corresponding author.

Acknowledgments

The authors thank Dentroid for providing the LED device for this study.

Conflicts of Interest

Laurence Walsh is the named inventor of the Nuralyte® LED device used in this study. Dentroid provided the LED device but had no role in study design, data collection, data analysis, interpretation of results, or preparation of the manuscript. No other conflicts of interest are declared.

Use of AI and AI-Assisted Technologies

No AI tools were utilized for this paper.

Abbreviations

ALP	Alkaline phosphatase
BMP-2	Bone morphogenetic protein-2
CCO	Cytochrome c oxidase
COL-1	Type I collagen
DMEM	Dulbecco's Modified Eagle's Medium
LED	Light-emitting diode
PMNI-LED	Multi-wavelength near-infrared LED
NIR	Near-infrared
OCN	Osteocalcin
OPN	Osteopontin
PBM	Photobiomodulation
PFA	Paraformaldehyde
ROS	Reactive oxygen species
RUNX2	Runt-related transcription factor 2

References

1. Berni, M.; Brancato, A.M.; Torriani, C.; et al. The Role of Low-Level Laser Therapy in Bone Healing: Systematic Review. *Int. J. Mol. Sci.* **2023**, *24*, 7094. https://doi.org/10.3390/ijms24087094.
2. Lima, A.M.C.T.; da Silva Sergio, L.P.; de Souza da Fonseca, A. Photobiomodulation via multiple-wavelength radiations. *Lasers Med. Sci.* **2020**, *35*, 307–316. https://doi.org/10.1007/s10103-019-02879-1.
3. Du, G.; Liu, M.; Qi, Y.; et al. BMP4 up-regulated by 630 nm LED irradiation is associated with the amelioration of rheumatoid arthritis. *J. Photochem. Photobiol. B Biol.* **2024**, *250*, 112828. https://doi.org/10.1016/j.jphotobiol.2023.112828.
4. Roberts, R.M.; Ezashi, T.; Temple, J.; et al. The role of BMP4 signaling in trophoblast emergence from pluripotency. *Cell. Mol. Life Sci.* **2022**, *79*, 447. https://doi.org/10.1007/s00018-022-04478-w.
5. Pan, Y.; Jiang, Z.; Ye, Y.; et al. Role and Mechanism of BMP4 in Regenerative Medicine and Tissue Engineering. *Ann. Biomed. Eng.* **2023**, *51*, 1374–1389. https://doi.org/10.1007/s10439-023-03173-6.
6. Amaroli, A.; Colombo, E.; Zekiy, A.; et al. Interaction between Laser Light and Osteoblasts: Photobiomodulation as a Trend in the Management of Socket Bone Preservation—A Review. *Biology* **2020**, *9*, 409. https://doi.org/10.3390/biology9110409.
7. Kulkarni, S.; Walsh, L.J.; Bhurani, Y.; et al. Assessment of the onset of analgesia and length of analgesia following the use of PBM with different wavelengths: A clinical study. *Lasers Med. Sci.* **2024**, *39*, 236. https://doi.org/10.1007/s10103-024-04184-y.
8. Tsai, S.R.; Hamblin, M.R. Biological effects and medical applications of infrared radiation. *J. Photochem. Photobiol. B Biol.* **2017**, *170*, 197–207. https://doi.org/10.1016/j.jphotobiol.2017.04.014.
9. Hamblin, M.R. Mechanisms and Mitochondrial Redox Signaling in Photobiomodulation. *Photochem. Photobiol.* **2018**, *94*, 199–212. https://doi.org/10.1111/php.12864.
10. Dedhar, S.; Mitchell, M.D.; Pierschbacher, M.D. The Osteoblast-Like Differentiated Phenotype of a Variant of Mg-63 Osteosarcoma Cell Line Correlated with Altered Adhesive Properties. *Connect. Tissue Res.* **1989**, *20*, 49–61. https://doi.org/10.3109/03008208909023874.
11. Staehlke, S.; Rebl, H.; Nebe, B. Phenotypic stability of the human MG-63 osteoblastic cell line at different passages. *Cell Biol. Int.* **2019**, *43*, 22–32. https://doi.org/10.1002/cbin.11073.
12. Hosseinpour, S.; Fekrazad, R.; Arany, P.R.; et al. Molecular impacts of photobiomodulation on bone regeneration: A systematic review. *Prog. Biophys. Mol. Biol.* **2019**, *149*, 147–159. https://doi.org/10.1016/j.pbiomolbio.2019.04.005.
13. Fávaro-Pípi, E.; Ribeiro, D.A.; Ribeiro, J.U.; et al. Low-Level Laser Therapy Induces Differential Expression of Osteogenic Genes During Bone Repair in Rats. *Photomed. Laser Surg.* **2011**, *29*, 311–317. https://doi.org/10.1089/pho.2010.2841.
14. Eslamian, L.; Ebadifar, A.; Mohebbi Rad, M.; et al. Comparison of Single and Multiple Low-Level Laser Applications After Rapid Palatal Expansion on Bone Regeneration in Rats. *J. Lasers Med. Sci.* **2020**, *11* (Suppl. S1), S37–S42. https://doi.org/10.34172/jlms.2020.s6.
15. Sleep, S.; Hryciw, D.; Gunter, J.; et al. Assessment of the influence of 660 and 808-nm PBM treatments on mitochondrial oxygen consumption of MG-63 osteoblast: A 3D cell culture study. *Lasers Med. Sci.* **2025**, *40*, 84. https://doi.org/10.1007/s10103-025-04349-3.

16. Sleep, S.; Gunter, J.; Hryciw, D.H.; et al. A 3D naive biological model for high-throughput live-cell analysis of mitochondrial oxygen consumption in response to photobiomodulation treatment. *Lasers Dent. Sci.* **2025**, *9*, 21. https://doi.org/10.1007/s41547-025-00296-y.
17. Sleep, S.L.; Ranjit, E.; Gunter, J.; et al. Mitochondrial Oxygen Consumption and Immunocytochemistry of Human Dental Pulp Stem Cell Following 808 nm PBM Therapy: A 3D Cell Culture Study. *J. Biophotonics* **2025**, *18*, e70051. https://doi.org/10.1002/jbio.70051.
18. Ranjit, E.; Hamlet, S.; Shelper, T.; et al. The effects of keratin-coated titanium on osteoblast function and bone regeneration. *Biomed. Mater.* **2024**, *19*, 035036. https://doi.org/10.1088/1748-605x/ad3f5f.
19. Schneider, C.A.; Rasband, W.S.; Eliceiri, K.W. NIH Image to ImageJ: 25 years of image analysis. *Nat. Methods* **2012**, *9*, 671–675. https://doi.org/10.1038/nmeth.2089.
20. Wiecheć, A.; Stodolak-Zych, E.; Frączek-Szczypta, A.; et al. The Study of Human Osteoblast-Like MG 63 Cells Proliferation on Resorbable Polymer-Based Nanocomposites Modified with Ceramic and Carbon Nanoparticles. *Acta Phys. Pol. A* **2012**, *121*, 546–550. https://doi.org/10.12693/aphyspola.121.546.
21. McDaniel, D.H.; Weiss, R.A.; Geronemus, R.G.; et al. Varying ratios of wavelengths in dual wavelength LED photomodulation alters gene expression profiles in human skin fibroblasts. *Lasers Surg. Med.* **2010**, *42*, 540–545. https://doi.org/10.1002/lsm.20947.
22. Amaroli, A.; Sabbieti, M.G.; Marchetti, L.; et al. The effects of 808-nm near-infrared laser light irradiation on actin cytoskeleton reorganization in bone marrow mesenchymal stem cells. *Cell Tissue Res.* **2021**, *383*, 1003–1016. https://doi.org/10.1007/s00441-020-03306-6.
23. Marques, M.M.; Diniz, I.M.A.; de Cara, S.P.H.M.; et al. Photobiomodulation of Dental Derived Mesenchymal Stem Cells: A Systematic Review. *Photomed. Laser Surg.* **2016**, *34*, 500–508. https://doi.org/10.1089/pho.2015.4038.
24. Yavagal, C.M.; Vikaraman, K.S.; Yavagal, P.C.; et al. Photobiomodulatory effects of multi wavelength diode lasers on the proliferation and differentiation of human dental pulp stem cells: An ex-vivo study. *Int. J. Health Sci.* **2022**, *6* (Suppl. S1), 2268–2279. https://doi.org/10.53730/ijhs.v6ns1.5164.
25. Luger, E.J.; Rochkind, S.; Wollman, Y.; et al. Effect of low-power laser irradiation on the mechanical properties of bone fracture healing in rats. *Lasers Surg. Med.* **1998**, *22*, 97–102. https://doi.org/10.1002/(sici)1096-9101(1998)22:2<97::aid-lsm5>3.0.co;2-r.
26. Huang, Y.Y.; Sharma, S.K.; Carroll, J.; et al. Biphasic dose response in low level light therapy—An update. *Dose Response* **2011**, *9*, 602–618. https://doi.org/10.2203/dose-response.11-009.hamblin.
27. Zhang, R.; Zhou, T.; Liu, L.; et al. Dose–effect relationships for PBM in the treatment of Alzheimer's disease. *J. Phys. D Appl. Phys.* **2021**, *54*, 353001. https://doi.org/10.1088/1361-6463/ac0740.
28. Chang, C.Y.; Aviña, A.E.; Chang, C.J.; et al. Exploring the biphasic dose-response effects of photobiomodulation on the viability, migration, and extracellular vesicle secretion of human adipose mesenchymal stem cells. *J. Photochem. Photobiol. B Biol.* **2024**, *256*, 112940. https://doi.org/10.1016/j.jphotobiol.2024.112940.
29. Sleep, S.L.; Walsh, L.J.; Zuaiter, O.; et al. PBM for dental analgesia and reversal from injected local anesthetic agents: A systematic review. *Lasers Dent. Sci.* **2024**, *8*, 52. https://doi.org/10.1007/s41547-024-00268-8.
30. Kulkarni, S.; George, R.; Love, R.; et al. Effectiveness of photobiomodulation in reducing pain and producing dental analgesia: A systematic review. *Lasers Med. Sci.* **2022**, *37*, 3011–3019. https://doi.org/10.1007/s10103-022-03590-4.
31. Pereira, D.A.; Mendes, P.G.J.; de Souza Santos, S.; et al. Effect of the association of infra-red and red wavelength photobiomodulation therapy on the healing of post-extraction sockets of third lower molars: A split-mouth randomized clinical trial. *Lasers Med. Sci.* **2022**, *37*, 2479–2487. https://doi.org/10.1007/s10103-022-03511-5.
32. Sama, M.V.; Kumar, P.M.; Penmetsa, G.S.; et al. Effect of Laser Photobiomodulation on Post-Surgical Healing, Implant Stability and Crestal Bone Levels around Implants: A Randomized Controlled Clinical Trial. *Int. J. Oral Maxillofac. Implant.* **2025**, 1–22. https://doi.org/10.11607/jomi.11568.
33. Chittabathina, P.; Gottumukkala, S.N.V.S.; Penmetsa, G.S.; et al. Clinical and microbiological outcomes of adjunctive photobiomodulation using various wavelengths in treatment of intrabony defects: A randomized controlled clinical trial. *Lasers Med. Sci.* **2025**, *40*, 471. https://doi.org/10.1007/s10103-025-04739-7.
34. Hamdy Ismail, H.; Obeid, M.F.; ElSaid Hassanein, E. The efficiency of single-session photobiomodulation on healing of periapical bone lesions using CBCT: A randomized clinical trial. *Lasers Med. Sci.* **2025**, *40*, 31. https://doi.org/10.1007/s10103-024-04242-5.